International Journal of Refrigeration 133 (2022) 181–190

Contents lists available at ScienceDirect

International Journal of Refrigeration

journal homepage: www.elsevier.com/locate/ijrefrig

Thermo-fluidic characteristics and performance in a distribute heating bubble pump generator

Caractéristiques et performances thermo-fluidiques dans un générateur avec pompe à bulle à chaleur distribuée

Honghai Yang [a,*], Yuping Chen [a], Yiwei Wu [a], Fengchang Yang [b], Xinyu Huang [a], Yue Xu [a], Wenli Duan [a]

[a] College of Environmental Science and Engineering, Donghua University, Shanghai 201620, China
[b] The State Key Laboratory of Nonlinear Mechanics, Institute of Mechanics, Chinese Academy of Sciences, Beijing 100190, China

ARTICLE INFO

Keywords:
Bubble pump generator
Distribute heating
Multiple lift tubes
Flow pattern evolution
Lift performance
Flow stability

Mots clés:
Générateur avec pompe à bulle
Chaleur distribuée
Tubes à élévations multiples
Évolution de la configuration d'écoulement
Performance d'élévation
Stabilité de l'écoulement

ABSTRACT

In some thermally driven two-phase natural circulation systems, bubble pumps serve as the key driving powers for the cycles. Recently a type of distribute heating bubble pump generator (BPG) is gradually receiving attention due to its compact structure and great potentials to utilize solar energy and low-grade waste heat recovery. The BPG provides a variety of promising features (e.g., passive heat transfer, enhanced reliability), which can benefit the advancing of heat transfer technology. For the primary study, we performed an experiment in a distributed heating BPG. Through utilizing multiple lift tubes and partial visualization configurations, it provides accesses to observe the flow pattern transition and monitor the flow instability, and thus to explore some of the underlying mechanisms affecting BPG performance.

Results showed that heat input and immersion height were crucial parameters to enable the operation of distribute heating BPG. With low heat input or high inlet water subcooling level, the flow within the pump was unstable with intermittent flow interruptions. As the heat input increased, the fluid flow became more stable, the vapor generation increased linearly, while the lifted liquid flow rate initially increased then decreased. Correspondingly, the flow pattern at the outlet section of lift tubes gradually changed from slug flow to churn flow, and then to annular flow. The higher of the immersion was, the higher heat input was needed for the flow pattern transition. It was in the churn flow regime at the outlet of lift tubes for the BPG to lift a maximum liquid. At lower immersion level, liquid reflux in the lift tubes was obvious and affected the flow stability as well as the lifting performance. At higher immersion level, the fluid flow was more stable and faster, which lifted more liquid while generated less vapor depending on the inlet subcooling. In general, the BPG showed better performance (both the lifted liquid and vapor generation increased) at smaller inlet subcooling level or lower system pressure. This study highlights the flow pattern evolution and flow stability, which is helpful to the reliable design and effective operation of the distributed heating BPG.

Introduction

In some thermally driven two-phase natural circulation systems, bubble pumps are used to replace mechanical pumps, and to lift liquid fluids from a reservoir in a low position to a vapor–liquid separator in a high position (Pfaff et al., 1998, Abu-Mulaweh et al., 2011, Kuo et al., 2013). The basic principle of bubble pumps is based on changes in the fluid density, especially refers to the case that the liquid fluid is partially vaporized and the resulting vapor bubbles lift the liquid (Pfaff et al., 1998, Abu-Mulaweh et al., 2011). With advantages such as no moving parts, stable, low noise, and electricity-free, the bubble pump shows great potentials in applications like electronic cooling (Abu-Mulaweh et al., 2011, Kuo et al., 2013), solar heating (Han-Shik et al., 2012, Jakob et al., 2007, Dammak et al., 2010) and solar cooling systems (Schmid and Spindler, 2016, Sayadi et al., 2013, Aman et al., 2019).

* Corresponding author.
E-mail address: yhh@dhu.edu.cn (H. Yang).

https://doi.org/10.1016/j.ijrefrig.2021.09.031
Received 12 April 2021; Received in revised form 16 September 2021; Accepted 26 September 2021
Available online 30 September 2021

Nomenclature

c_p	specific heat at constant pressure (kJ kg^{-1} K^{-1})
d	diameter (mm)
H	height (mm)
h	enthalpy (kJ kg^{-1}), height (m)
h_{LV}	latent heat of vaporization (kJ kg^{-1})
L	length (m)
$\dot{m}$	transient mass flow rate (kg h^{-1})
$\overline{m}$	average mass flow rate (kg h^{-1})
N	number of recorded data
Q	heat input (W)
P	pressure (Pa)
R	derived quantity
T	temperature (°C)
x	vapor quality, measured quantity

Greek letters

ρ	density (kg m^{-3})
σ	surface tension (N m^{-1})
τ	time (s)
Δ	difference
δ	deviation

Subscripts

BPG	bubble pump generator
cal	calculation
el	electrical
eq	equipment
exp	experiment
in	inlet
L	liquid
loss	heat loss
lt	lift tube
max	maximum
me	measurement
out	outlet
sat	saturate
sub	subcooling
sys	system
V	vapor

In terms of different heating types, the configuration of a bubble pump can be typically set to a spot heating mode or a distribute heating mode (Siyoung et al., 1998, Garma et al., 2014, Bierling et al., 2019). Most conventional bubble pumps usually adopt the spot heating mode, which consists of a base generator and adiabatic lift tubes. This operation mode enables higher pumping rates and a conceptually simple approach for the vapor separation and fluid circulation but usually requires either a higher heat flux or higher heating source temperature to transfer heat over a smaller area (Bierling et al., 2019, Rattner and Garimella, 2015). In contrast, the distribute heating mode typically uses lift tubes, which are heated along the entire length and served as the generator/riser simultaneously. This type of bubble pump is usually called a distribute heating bubble pump generator (BPG). Due to larger heat transfer area in BPG, the required heat flux is much lower compared to that of the spot heating mode. Hence, it enables operation with relatively low temperature or waste heat sources and also gives greater flexibility in inventing a more compact and efficient machine (Jakob et al., 2007, Schmid and Spindler, 2016, Rattner and Garimella, 2015, Zhang et al., 2006). It has been widely recognized that, depending on heating types and the heat flux, the gradient in density, vapor quality and flow patterns in lift tubes vary (Abu-Mulaweh et al., 2011, Bierling et al., 2019, Aman et al., 2018, Gartia et al., 2006, Benhmidene et al., 2011), which in turn lead to different flow and heat transfer mechanisms (Gartia et al., 2006, Franco and Filippeschi, 2013, Rattner and Garimella, 2018, Trinh et al., 2019). Analysis of operation in such distribute heating BPG usually encounters additional challenges, because the liquid and vapor flow rates and patterns evolve along the entire tube length and are not same as that at the inlet, which are typically assumed for spot heating configurations (Rattner and Garimella, 2015, Trinh et al., 2019).

Currently, there only exists limited researches focusing on the distribute heating BPG. However, it is gradually receiving attention under the progress of worldwide energy and environmental sustainability attributing to its unique advantages in the applications of solar energy and low-grade waste heat recovery (Jakob et al., 2007, Dammak et al., 2010, Rattner and Garimella, 2015, Zhang et al., 2006, Benhmidene et al., 2016). Jakob et al. (Jakob et al., 2007) developed a vertical shell-and-tube coupling-fluid-heating BPG for a residential-scale solar heat driven ammonia/water diffusion absorption refrigeration air-conditioning system. They described five design iterations, which attests to the difficulty of designing a BPG to operate in this distribute heating mode. However, detailed BPG models and performance results were not reported. Zhang et al. (2006) proposed a distribute heating BPG with the lunate channel and investigated experimentally with LiBr–H_2O solution. They found the lunate channel showed several outstanding characteristics, such as low starting temperature (minimum 68 °C), wide operating temperature range and lower requirement for vacuum condition (under 10 kPa). Rattner and Garimella (2015) investigated a co-flow upward tube-in-tube distribute heating BPG, where water-steam was used as the working fluid and flowing in the inner lift tube (inner diameter 7.8 mm), while a mineral oil was used as the heating fluid and circulated in the annulus. They found this configuration could operate with thermal input as low as 11 °C above the fluid saturation temperature. Also, a detailed mechanistic coupled fluid flow and heat transfer model was developed and validated for their BPG design. This investigation demonstrated that coupling-fluid heated BPG was a promising alternative to conventional spot-heated implementations and could enable refrigeration using low-grade thermal energy. Benhmidene et al. (2016) tested a coaxial double-tube bubble pump with ammonia/water as the working fluid. Heating power and submersion ratio (the ratio of immersion height H with the lift height L, as shown in Fig. 1) were changed to affect the bubble pump performance, such as the average mass flow rate of solution and refrigerant. In order to analyze the flow stability, pressure oscillation was measured in the separator and reservoir.

As for the numerical studies, some investigations were tried to simulate the flow boiling of the distribute heating BPG to predict the void fraction distribution, flow regime repartition, liquid-vapor velocities evolution, and pressure drop, etc. (Garma et al., 2014, Gartia et al., 2006, Benhmidene et al., 2011, Jo et al., 2014). Since the two-phase flow with the boiling phase change process inside the BPG is extremely complex, techniques for simulating two-phase flows with phase-change heat transfer are still in their infancy (Rattner and Garimella, 2018). It is typically difficult to accurately describe the pumping performance of the BPG by numerical simulation and, therefore, experimental test is still the most effective way to study BPG so far (Han et al., 2015).

In summary, the studies on the bubble pump are still in the primary stage, especially for the distributed heating mode. Moreover, rather few research revealed the flow instability in the bubble pump, which is an inherent characteristic of the two-phase natural circulation (Franco and Filippeschi, 2013, Koyfman et al., 2003, Ben Ezzine et al., 2010), and

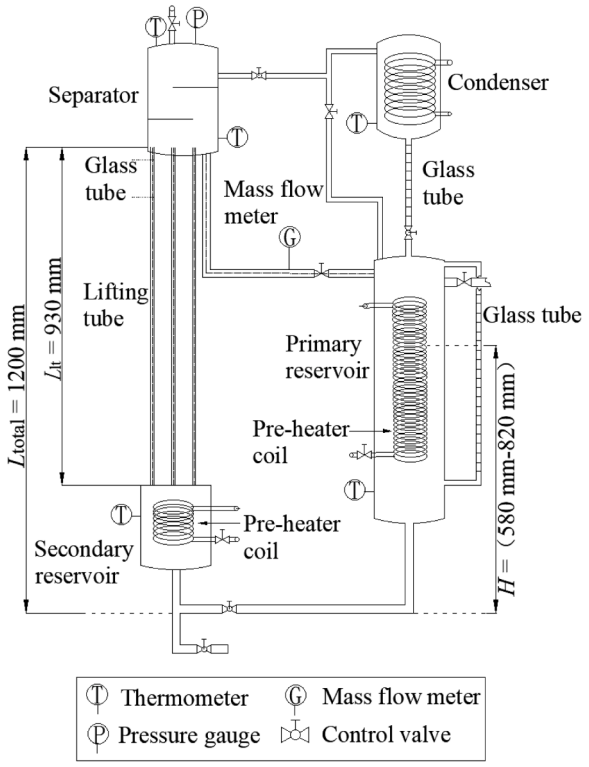

Fig. 1. Schematic diagram of the experimental set-up.

may be a new subject of research (Benhmidene and Chaouachi, 2019). Hence, it is important to study and understand this issue, which will assist the future design of BPG by knowing the bubble pump functioning and their optimum operation conditions in which the instability is minimal (Benhmidene and Chaouachi, 2019).

In order to reveal the flow behavior and characteristics of the distribute heating BPG, a test rig with multiple lift tubes and partial visualization constructs was set up and investigated in this paper. During the experiments, geometric parameters were kept constant, while operational parameters were varied, such as the heating input, immersion height, inlet sub-cooling temperature, and the system pressure. Flow pattern evolution and flow instability were detected and analyzed, as well as the pumping performance under the effects of operational conditions through the flow visualization and transient fluid flow measurement.

Experimental apparatus and methods

2.1. Experimental setup

Fig. 1 shows the experimental apparatus, which consists of the lifting tubes, separator, condenser, primary and secondary reservoirs, etc. The working principle of this experimental apparatus is similar to previous BPG experiments (Bierling et al., 2019, Rattner and Garimella, 2015, Zhang et al., 2006): as the working fluid is heated in the lifting tubes, its temperature rises gradually to a boiling point, then the working fluid begins to boil and generate a great number of bubbles. When the boiling two-phase fluid rises to the vapor–liquid separator, the liquid goes back through a pipe to the primary reservoir, while the vapor flows to the condenser, and is cooled back to the liquid, then flows into the primary reservoir. At last, the liquid in the primary reservoir flows down to the secondary reservoir with the thermosyphon action to complete an operation cycle.

As for the geometric size of the BPG, previous studies showed that tube diameter and lift length are critical parameters (Pfaff et al., 1998, Abu-Mulaweh et al., 2011, Jakob et al., 2007, Siyoung et al., 1998, Bierling et al., 2019, Belman-Flores et al., 2014, Delano, 1998). It is generally thought the bubble pump operates most efficiently in the slug flow regime in which the vapor bubbles are approximately the diameter of the tube (Delano, 1998, White, 2001). There is a maximum tube diameter above which slug flow will not occur is predicted by Chisholm (1985) correlation,

$$d_{\max} = 19\sqrt{\frac{\sigma}{g(\rho_L - \rho_V)}} \tag{1}$$

It is true that widening tube diameter could lead to reduction of the friction factor, thereby increasing the flow rate through the bubble pump. However, excessively tube diameter or lifted height would cause pumping action to stop (Pfaff et al., 1998, Siyoung et al., 1998). According to the previous studies, the normal ranges were 5–14 mm for the inner diameter and 0.2–2.0 m for the lift length (Pfaff et al., 1998, Siyoung et al., 1998, Bierling et al., 2019, Belman-Flores et al., 2014, Delano, 1998, White, 2001). In current study, we chose 8 mm for the inner diameter and 930 mm for the lift tube length and kept them constant during the experiments.

Moreover, multiple lift tube configurations were adopted in the literature (Lin et al., 2016, Vicatos and Bennett, 2007, Gurevich et al., 2015). Their results indicated that increasing the number of lift tubes could boost the pump's ability to handle larger heat loads and flow rates. Meanwhile, multi-tubes design could lead to the problem of unequal flow distribution, *i.e.,* mal-distribution phenomenon (O'Neill and Mudawar, 2020, Ham et al., 2021, Ruspini et al., 2014). In a guided bubble pump with multiple tubes, Lin et al. (2016) found different flow patterns in each riser, from bottom to top, especially when the heat input was lower. Overall, the flow regime was basically slug flow within their experimental conditions. In another reference, Gurevich et al. (2015) found that mutual influence between the tubes was negligible, *i.e.*, flow rates were evenly distributed among the tubes. For these above references (Lin et al., 2016, Vicatos and Bennett, 2007, Gurevich et al., 2015), spot heating modes were adopted and the working fluid was water-steam in references (Lin et al., 2016, Vicatos and Bennett, 2007) and R134a-DMAC (organic binary solution) in reference (Gurevich et al., 2015). Here, three parallel stainless pipes were adopted as lift tubes, and uniformly heated along the tube length through three glass fiber heating belts. Water-steam was used as the working fluid for primary study. For visualization of flow patterns, the exit section of one lift tube was made of transparent quartz glass with a length of 80 mm without heating. Also, the same sections of another two stainless tubes were unheated during the experiment. To minimize heat loss from the test section, each tube was wrapped with 15 mm thick glass wool insulation, then the whole assembly was insulated with a 50 mm thick glass wool jacket and covered with aluminum foils. The indoor air temperature was kept around 26 ±0.5 °C through the air conditioner, thus the total heat loss was evaluated less than 6.8%. Moreover, two large cylinder reservoirs with the inner diameter of 150 mm were employed to reduce fluctuations in the immersion height during the experiments.

2.2. Experimental methods

During the experiments, the total lift height (L_{total} = 1.2 m, includes the length of lift tube and the height of the secondary reservoir, *etc.*, as shown in Fig. 1) was kept constant, while the immersion height (H, the height of the liquid level in the primary reservoir, as shown in Fig. 1) was changed in the range of 580–820 mm, and obtained through measuring the liquid level height in a glass tube, which was bypass connection to the primary reservoir. Heat input to the lifted tubes was varied in the range of 185–900 W. The inlet subcooling temperature of the liquid into the lift tubes ΔT_{sub} was controlled by the pre-heater coils in two reservoirs and changed within the range of 8 to 45 °C with a

temperature step of 7–10 °C. Before charging the system with the working fluid (*i.e.*, deionized water in this experiment), the system was evacuated using a vacuum pump. Then the fluid was heated in order to minimize the amount of non-condensable gases dissolved inside, as similar as in the reference (Franco and Filippeschi, 2013). During the experiment, the system pressure could be changed in the range of 60 kPa to 100 kPa with a pressure step of 10 kPa.

The transient liquid lifted mass flow rate $\dot{m}_{L,out}$ was measured continuously by a Coriolis mass flow meter, while the average value $\overline{m}_{L,out}$was calculated in the period of quasi-steady state (about 40 minutes was continued). The average vapor generation rate $\overline{m}_V$was measured indirectly through the condensate water using the following method: once the system reached in quasi-stable state, the valve below the condenser was turned off, then the condensate water would accumulate in a glass tube (which is installed between the condenser and the primary reservoir) for a short period of time. After a certain volume of liquid was collected, the amount of the condensed water was divided by the recorded time to calculate the average condensate water flow rate, which is considered equal to $\overline{m}_V$. This process was repeated four times to reduce measurement errors. A high-accuracy data acquisition logger (Agilent-Technologies, 34970A) was used to collect the temperature, pressure at a frequency of 1 Hz with the uncertainty of ±[0.0035 % •reading + 0.0005 % • range].

Data reduction

3.1. Control volume analysis

Fig. 2 shows a control volume including the lifted tubes and the separator. Mass balance and energy conservation equations for this control volume observe following equations,

$$\dot{m}_{L,in} = \dot{m}_{L,out} + \dot{m}_V \tag{2}$$

$$\dot{Q}_{BPG} = \dot{m}_{L,out}\cdot h_{L,out} + \dot{m}_V\cdot h_V - \dot{m}_{L,in}\cdot h_{L,in} \tag{3}$$

where, $\dot{Q}_{BPG}$ is the supplied heat flow to the BPG, and can be calculated as

$$\dot{Q}_{BPG} = \dot{Q}_{el} - \dot{Q}_{loss} \tag{4}$$

where, $\dot{Q}_{el}$is the electrical power to the lift tubes, and $\dot{Q}_{loss}$ is the heat loss from the control volume.

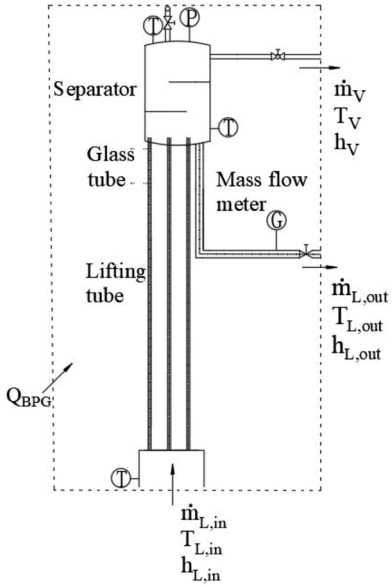

Fig. 2. Control volume analysis of the BPG.

Substituting Eq. (2) into Eq. (3) results in

$$\dot{Q}_{BPG} = \dot{m}_{L,in}\left(h_{L,out} - h_{L,in}\right) + \dot{m}_V\left(h_V - h_{L,out}\right) \tag{5}$$

Assuming the outlet water and steam in saturate state, i.e.

$$T_{L,out} = T_V = T_{sat} \tag{6}$$

Thus, we can have

$$\begin{aligned}\dot{Q}_{sensible} &= \dot{m}_{L,in}\left(h_{L,out} - h_{L,in}\right)\\ &= \dot{m}_{L,in}\cdot\overline{c}_{pL}\Big|_{T_{L,in}}^{T_{sat}}\cdot\left(T_{sat} - T_{L,in}\right)\\ &= \dot{m}_{L,in}\cdot\overline{c}_{pL}\Big|_{T_{L,in}}^{T_{sat}}\cdot\Delta T_{sub}\end{aligned} \tag{7a}$$

$$\dot{Q}_{latent} = \dot{m}_V\left(h_V - h_{L,out}\right) = \dot{m}_V\cdot h_{LV} \tag{7b}$$

where $\dot{Q}_{sensible}$ and $\dot{Q}_{latent}$are the sensible and latent heat of the control volume respectively, ΔT_{sub} is the inlet subcooling of temperature of the liquid into the lift tubes, h_{LV} is the latent heat of vaporization. Thus, Eq. (5) can be rewritten as

$$\begin{aligned}\dot{Q}_{BPG} &= \dot{Q}_{sensible} + \dot{Q}_{latent}\\ &= \dot{m}_{L,in}\cdot\overline{c}_{pL}\Big|_{T_{L,in}}^{T_{sat}}\cdot\Delta T_{sub} + \dot{m}_V\cdot h_{LV}\end{aligned} \tag{8}$$

For the average in the period of quasi-stable state, we can obtain

$$\overline{Q}_{BPG} = \overline{m}_{L,in}\cdot\overline{c}_{pL}\Big|_{T_{L,in}}^{T_{sat}}\cdot\Delta T_{sub} + \overline{m}_V\cdot h_{LV} \tag{9}$$

Neglecting the variation of heat input with the time, then

$$\dot{Q}_{BPG} = \overline{Q}_{BPG} = Q_{BPG} \tag{10}$$

Substituting Eq. (2) into Eq. (9), we have

$$Q_{BPG} = \overline{m}_{L,out}\cdot\overline{c}_{pL}\Big|_{T_{L,in}}^{T_{sat}}\cdot\Delta T_{sub} + \overline{m}_V\cdot\left(\overline{c}_{pL}\Big|_{T_{L,in}}^{T_{sat}}\cdot\Delta T_{sub} + h_{LV}\right) \tag{11}$$

From Eq. (11), can obtain that

$$\overline{m}_V = \frac{Q_{BPG} - \overline{m}_{L,out}\cdot\overline{c}_{p,L}\Big|_{T_{L,in}}^{T_{sat}}\cdot\Delta T_{sub}}{\overline{c}_{pL}\Big|_{T_{L,in}}^{T_{sat}}\cdot\Delta T_{sub} + h_{LV}} \tag{12}$$

In the case of $T_{L,in} = T_{sat}$, namely when $\Delta T_{sub} = 0$, we have

$$\overline{m}_V = \frac{Q_{BPG}}{h_{LV}} \tag{13}$$

The average vapor quality of the two-phase mixture at the exit of test section is defined as

$$\overline{x} = \frac{\overline{m}_V}{\overline{m}_V + \overline{m}_{L,out}} \tag{14}$$

From Eqs. (12-13) we can calculate the average vapor generation rate $\overline{m}_V$, as the other parameters in the equation are known through the measurement, such as Q_{BPG}, $\overline{m}_{L,out}$, $T_{L,in}$, and T_{sat}, etc. In this experiment, P_{sys} is the measured vapor pressure in the separator and can be used to obtain the value of T_{sat}, and h_{LV}. Thermophysical properties of water-steam can be taken from the REFPROP program developed by NIST (Lemmon et al., 2018) and from the ASHRAE Handbook Fundamentals (Handbook-Fundamentals, 2009).

When the subcooling water flows in the lift tubes, the total pressure drop accounts for both single-phase and two-phase flow regions, including the hydrostatic (gravitational) pressure drop, frictional pressure drop, and momentum (acceleration) pressure drop (for the single-phase flow, the acceleration pressure drop is zero due to no vapor formation) (Trinh et al., 2019). Rattner and Garimella (2015) demonstrated that, for the BPG, the hydrostatic (gravitational) pressure drop was the dominant component, while the net pressure drop due to fluid acceleration was quite small. Based on the basic pressure drop theory of

two-phase flow and the pressure drop balance theory of the system (Bierling et al., 2019, Franco and Filippeschi, 2013, Lin et al., 2016), the total pressure drop in the lift tubes is evaluated in the range of 3.0–5.5 kPa for the present experimental set-up. Considering that the system pressure changed in the range of 60 kPa to 100 kPa, we neglect the influence of pressure drop on the change of thermophysical properties along the lift tubes for the simplicity of analysis, in addition, we take $\bar{c}_{pL}|_{T_{L,in}}^{T_{sat}} = 4.2\text{kJ}\cdot(\text{kg}\cdot^{\circ}\text{C})^{-1}$ for all cases in this experiment.

On the other hand, we can measure the $\overline{m}_V$ indirectly through the condensate water in this experiment. Therefore, we can compare the calculated $\overline{m}_V$ and the measured $\overline{m}_V$, as shown in Fig. 3. Their root mean square error (RMS) (Gartia et al., 2006) is about 14.6% for all measured data. Heat losses, influence of pressure drop on the change of thermophysical properties, and uncertainties in the measurement, such as the $\overline{m}_{V,exp}$, $\overline{m}_{L,out}$, and ΔT_{sub}, etc. were responsible for this discrepancy between the experiment and calculation.

3.2. Uncertainty analysis

For a measured quantity x, the uncertainty can be calculated by Eq. (15) (Moffat, 1988):

$$\delta x = \sqrt{\delta x_{eq}^2 + \delta x_{me}^2} \tag{15}$$

where δx_{eq} is the uncertainty of the equipment, as listed in Table 1, δx_{me} is the uncertainty of the measurement.

For a derived quantity R, the uncertainty can be calculated by Eq. (16) (Moffat, 1988):

$$\delta R = \sqrt{\sum_{i=1}^{N}\left(\frac{\partial R}{\partial x_i}\delta x_i\right)^2} \tag{16}$$

where δR is the uncertainty of derived quantity R, x_i is the independent variable of R, δx_i is the uncertainty of x_i.

Table 2 gives the maximum uncertainties of main parameters in this study. Here heat loss is included in the uncertainty estimation of Q_{BPG}. The uncertainty of the saturation temperature T_{sat} is estimated from the uncertainty of P_{sys}. As to the uncertainty of inlet subcooling ΔT_{sub}, influence of pressure drop in the lift tubes is considered. For the average vapor generation rate $\overline{m}_V$, it is measured indirectly through the condensate water, thus its maximum uncertainty is estimated about 3.2% when considering the possible error on the time measurement and on the volume collected.

It is worth to mention that the liquid mass flow rate is measured directly in this experiment and found to fluctuate continually even in the quasi-steady state, as observed in the references (Bierling et al., 2019, Koyfman et al., 2003). Therefore, when the system reaches a quasi or pseudo-steady state at each stage, it continues about 40 min to measure the transient liquid mass flow rate and then to calculate the average liquid mass flow rate in following way:

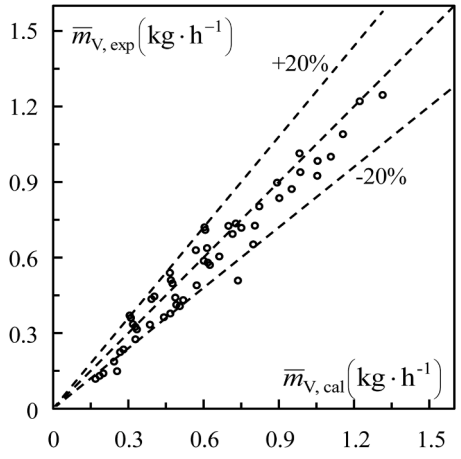

Fig. 3. Comparison of the measured and calculated vapor mass flow.

Table 1
Specification of measuring equipment.

Parameters	Measuring equipment	Measured range	Uncertainty
Temperature	Thermocouple, K-type, ø0.2 mm	20–120 °C	0.2 °C
Pressure	UNIK5000	0–1.5 bar	0.04%FS
Flow Rate	DMF-1 -1-A Mass flow meter	0–20 kg h^{-1}	0.15%FS
Power	Everfine-PF9901 Electronic power meter	0–1000 W	2 W
Time	Stopwatch	15 min	0.1 s

Table 2
Maximum uncertainties of main parameters.

Parameters	Maximum uncertainties (%)
H	0.2%
P_{sys}	0.3%
ΔT_{sub}	14.2%
Q_{BPG}	7.4%
$\overline{m}_V$	3.2%
$\overline{m}_{L,out}$	2.8%

$$\overline{m}_{L,out} = \frac{\sum_{i=1}^{N}\dot{m}_{L,out}}{N} \tag{17}$$

where, N is the number of recorded data, which is about 2300–2400.

The standard square deviation is determined by Eq. (18) (Yeboah and Darkwa, 2018, Halimi et al., 2017):

$$\delta = \sqrt{\frac{\sum_{i=1}^{N}\left(\dot{m}_{L,out} - \overline{m}_{L,out}\right)^2}{N}} \tag{18}$$

The standard error of $\overline{m}_{L,out}$ is determined by Eq. (19) (Yeboah and Darkwa, 2018, Halimi et al., 2017):

$$\delta_{me} = \frac{\delta}{\sqrt{N}} \tag{19}$$

Table 3 lists the time-average liquid mass flow rate $\overline{m}_{L,out}$, the standard deviation δ and the standard error δ_e for some representative cases.

In order to verify the repeatability of experiments, a typical working condition ($P_{sys} = 100\,\text{kPa}, H = 660\,\text{mm}, \Delta T_{sub} = 15\,^{\circ}\text{C}$) was performed three times. Results showed that the standard error of $\overline{m}_{L,out}$ for each heat input was less than 2%. This guarantees the validity of the attained results.

4.1. Effect of heat input

In this study, inlet subcooling of the lift tubes and system pressure were kept constant, *i.e.*, $p_{sys} = 100\,\text{kPa}, \Delta T_{sub} = 15\,^{\circ}\text{C}$, while immersion height (H) was kept at 580 mm, 660 mm, 740 mm, and 820mm respectively.

Fig. 4 shows the influence of heat input on the average liquid lifting rate ($\overline{m}_{L,out}$) and average vapor generation rate ($\overline{m}_V$) respectively. At lower immersion height (*e.g.*, 580 mm and 660 mm), the liquid lifting rate first increases with the heat input, then reaches a maximum value at about 530–600 W, after which it decreases moderately. Similar results were reported in previous studies, both in the spot and distribute heating modes Franco and Filippeschi, 2013, Benhmidene et al., 2016, Delano, 1998, Lin et al., 2016). The flow pattern transitions with the heat fluxes

Table 3
$\overline{m}_{L,out}$, standard deviation δ and error δ_{me} for some representative cases.

	Q_{BPG} (W)	H (mm)	ΔT_{sub} (°C)	P_{sys} (kPa)	$\overline{m}_{L,out}$ (kg•h^{-1})	δ (kg•h^{-1})	δ_{me} (kg•h^{-1})	$\delta_{me}/\overline{m}_{L,out}$ (%)
1	185	580	15	100	1.62	0.494	0.01	0.63
2	600	580	15	100	4.01	0.332	0.007	0.17
3	800	580	15	100	3.15	0.216	0.004	0.14
4	530	580	15	100	3.93	1.296	0.027	0.68
5	530	740	15	100	9.21	0.580	0.011	0.13
6	310	660	8	100	6.47	0.61	0.013	0.19
7	310	660	35	100	3.42	0.88	0.018	0.53

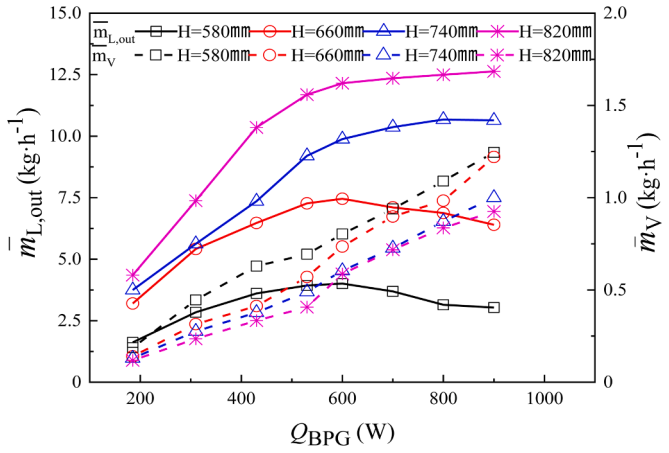

Fig. 4. Effect of heat input on the BPG performance (P_{sys} = 100 kPa, ΔT_{sub} = 15 °C)

were their common views (Aman et al., 2018, Franco and Filippeschi, 2013, White, 2001). At higher immersion height (e.g., 740 mm and 820 mm), no late decrease of $\overline{m}_{L,out}$ as a function of heat input was observed. However, the curve tends to increase slowly only at higher heating power. This observation means even though the maximum liquid lifted rate may be corresponding to heat input over 900 W (the maximum permitted electrical heat input was 1000 W in this experiment), but its upside was limited. As to the variation of vapor generation rate, it increases nearly in linear as the heat input increases, which can be demonstrated by Eqs. (12-(13).

Fig. 5 shows the flow pattern evolution at the outlet section of a lift tube (H = 660 mm). At lower heat input, e.g., 185 W, less vapor was generated and rose slowly. Accordingly, an obvious slug flow was observed (characterized by a clear and round head of the bubble), meanwhile less liquid was lifted in this case. With the increase of heat input, e.g., 310 W and 430 W, more vapor was generated and rose faster. Vapor bubbles became deformed and tended to break, accompanied by the oscillation of liquid columns, which means the transition of flow pattern. Further increasing the heat input to 530 W and 600 W, an obvious churn flow was observed at the outlet of the lift tube, corresponding to a maximum ability to lift the liquid (see Fig. 4). Continuing to increase the heat input to 700 W - 900 W, the vapor production increased sharply with an extremely fast flow up, leading to a wavy flow of the vapor–liquid interface accompanied with more liquid sucked into the gaseous core. This observation means the flow pattern converted to annular flow gradually, while the liquid lifted rate decreased again. Similar flow pattern evolution could be observed at other immersion heights. The higher of the immersion was, the higher heat input was needed for the flow pattern transition.

Normally, the slug flow regime is considered as the optimal operation condition for lifting liquid and under which the BPG operates most efficiently (Pfaff et al., 1998, Abu-Mulaweh et al., 2011, Siyoung et al., 1998, Delano, 1998, White, 2001). It is typically true for the spot heating BPG, where the working fluid is only heated in the base generator to produce bubbles, while it is usually adiabatic in vertical lift tube. Thus, the flow pattern is unchanged in the lifting process, *i.e.*, it maintains bubbly flow, slug flow, churn flow, or annular flow, respectively depending on the vapor production from the base generator and the inner diameter of the lift tube (Pfaff et al., 1998, Abu-Mulaweh et al., 2011, Bierling et al., 2019). However, it is not the same situation for the distribute heating BPG in which the lift tube is heated along the entire length serving as the generator and riser simultaneously. Thus, the working fluid was uniformly heated in the vertical lift tube and bubbles generated at the inner surface of tube walls, which is commonly called flow boiling, and the flow pattern evolves along the entire tube length undergoing the single-phase liquid flow, bubbly flow, slug flow, churn flow, and annular flow. Therefore, the two-phase flow in the distribute

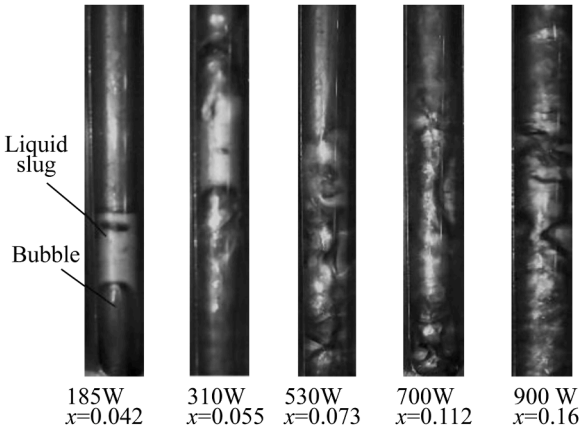

Fig. 5. Flow patterns evolution with the heat input (8 mm × 80 mm for each size (P_{sys} = 100 kPa, H = 660 mm, ΔT_{sub} = 15 °C)

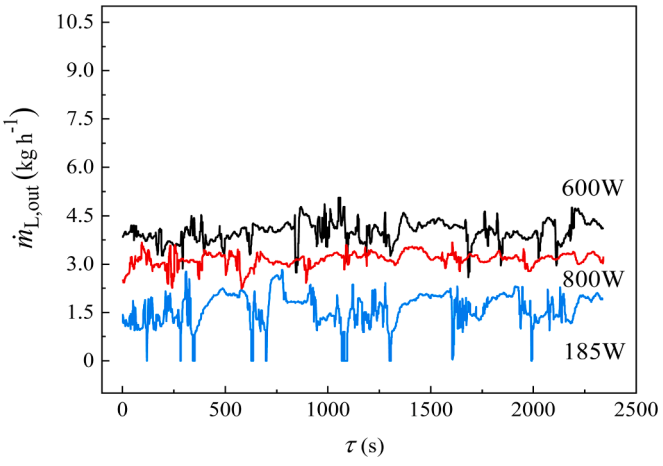

Fig. 6. Transient liquid lifted flow rate at different heat inputs (P_{sys} = 100 kPa, H = 580 mm, ΔT_{sub} = 15 °C).

heating mode is more complex than in the spot heating mode (Jakob et al., 2007, Zhang et al., 2006, Benhmidene et al., 2011). In the current experiments, the maximum lift ability occurred as the fluid at the outlet of the lift tube was in transition from slug to churn flow.

Fig. 6 shows the transient liquid lifted mass flow rate $\dot{m}_{L,out}$ at different heat inputs (H=580 mm). At lower heat input, e.g., 185 W, the fluid flow was unstable with drastic fluctuation and sometimes even flow stagnation occurred. By increasing the heat input, the fluid fluctuation became more moderate and the average liquid lifting rate reached a peak at 600 W, then decreased again as heat increased (e.g., 800 W).

Also, an aperiodic oscillating flow was observed versus time which confirms the pumping instability along the bubble pump. Overall, the frequency of oscillation increased while the amplitude decreased with the increase of the heat input, which is corresponding to the flow pattern transition. In fact, the periodic pumping of the working fluid is a characteristic of the bubble pump, and the fluid flows occasionally in intermediate pulsation or chaotic modes (Bierling et al., 2019, Benhmidene et al., 2016), which can be attributed to the inherent instability of the two-phase natural circulation (Franco and Filippeschi, 2013, O'Neill and Mudawar, 2020, Ruspini et al., 2014). Generally, the instabilities caused by two-phase flow instabilities with boiling are either static instabilities, induced by a steady-state boiling process which mainly includes Ledinegg instability, or dynamic instabilities initiated by transient changes in the boiling process. Dynamic instabilities include mainly density wave oscillations, pressure drop and thermal oscillations, *etc.* Instabilities of flow pattern transition and parallel channel may refer to either static or dynamic phenomenon (O'Neill and Mudawar, 2020, Ruspini et al., 2014).

Several factors can cause flow oscillation in the bubble pump. For example, when the variation of pressure drop *vs* mass flux is presented in N-shape curve, it can cause an oscillation phenomenon in the bubble pump (Benhmidene and Chaouachi, 2019). Heat supplied to the bubble results in a flow regime transition and it can cause flow oscillation in addition to thermal oscillation, as observed in present experiments. In addition, parallel lift tubes may lead to the static instability (*i.e.*, flow mal-distribution, due to Ledinegg) and dynamic instability (due to interacting density wave oscillations across channels) (O'Neill and Mudawar, 2020, Ruspini et al., 2014). Indeed, the flow instability in the bubble pump is important to its reliable and effective operation, while it is a rather complicated issue and need to be further investigated.

As for the optimal value of heat input, it is known relating to the flow pattern transition and also dependent on the submergence ratio (H/L), tube diameter and working fluid properties, etc. (Benhmidene et al., 2016, Delano, 1998, Benhmidene et al., 2011). In this study, the optimal heat input value increased as the immersion height increased, as shown in Fig. 5. This trend was likely due to the fact that, when the heat input and inlet subcooling were fixed, a higher immersion led to a faster liquid mass flow rate and a smaller vapor generation rate (see Fig. 7 in Section 4.2 for details), which led to the delay of flow pattern evolution. Rationally, the higher heat input and lower level of inlet subcooling are expected to generate more vapor and accelerate the flow pattern transition. However, there only existed scarce studies that focused on this issue to our best knowledge, and worth to be further investigated for the purpose of proper design and effective operation of the BPG.

4.2. Effect of immersion height

In this section, the inlet subcooling of lift tubes and the system pressure were kept constant, *i.e.*, $\Delta T_{sub} = 15\,^{\circ}C$, $P_{sys} = 100\,kPa$while the effect of immersion height was studied.

Fig. 7 shows that, for a given heat input, increasing the immersion height leads to the significant increase of the lifted liquid flow rate, but also a slight decrease in the vapor generation rate. It can be understood as follows: under a higher immersion, a larger driving force was generated through the thermosyphon action, while a shorter distance (L-H) was lifted for the liquid to the separator, both them were contributing to a higher circulating velocity, leading to a faster liquid flow, thus both $\dot{m}_{L,in}$and$\dot{m}_{L,out}$increased (Koyfman et al., 2003, Chan and McCulloch, 2013). In addition, the flow within the lift tube became more stable at the higher immersion, as shown in Fig. 8. On the other hand, when the total heat input and inlet subcooling were fixed, more liquid flow consumed additional sensible heat, leading to the reduction of amount of latent heat transfer, and thus less vapor was generated, as demonstrated in Eq. (12).

Moreover, Eq. (13) indicates that in the case of $\Delta T_{sub} = 0$, *i.e.*, when the inlet liquid is in the saturated state, no sensible heat is consumed in the BPG. Consequently, all heat input is used for vapor generation. This result means the vapor generation rate will be constant for a fixed heat input value and not being affected by the variation of the submergence height.

During the experiment, a certain liquid re-flux phenomenon was observed at the outlet of the lift tube. Actually, in the distribute heating BPG, the liquid lifting process is similar to a rising relay (as a bubble plug rises in the lift tubes, it also pushes its forehead liquid column up). However, when the bubble breaks up, it sometimes leads to a short period of the back-flow of the liquid, which is then again pushed to a higher position by the next bubble plug. A similar process is repeated several times until finally the liquid column rises to the separator. At lower immersion, longer distance is lifted for the liquid to the separator, which means more bubble plugs break up in the rising process, leading to more liquid re-flux affecting the flow stability and lifted liquid flow

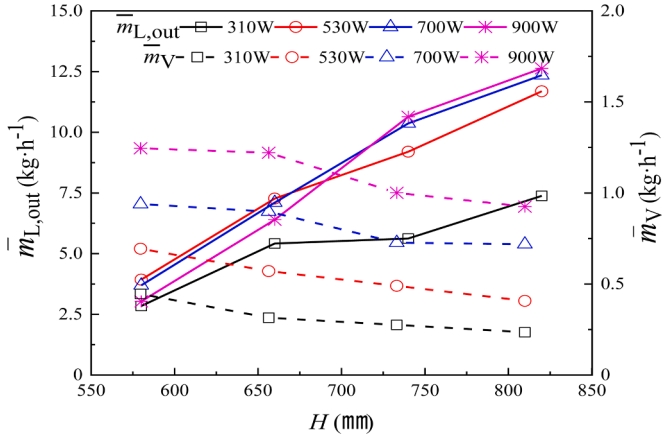

Fig. 7. Effect of immersion height on the BPG performance (P_{sys} = 100 kPa, ΔT_{sub} = 15 °C).

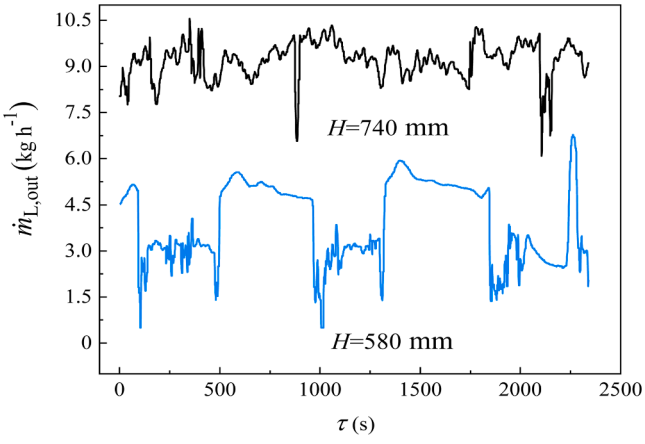

Fig. 8. Transient liquid lifted rate at different immersion height (P_{sys} = 100 kPa, ΔT_{sub} = 15 °C, Q_{BPG} = 530 W)

rate, as demonstrated in Fig. 8. Moreover, the oscillation frequency of liquid flow increases while the amplitude decreases with the increase of immersion height.

4.3. Effect of inlet subcooling level

In this section, the immersion height and system pressure were kept constant, *i.e.*, H=660 mm, P_{sys} = 100 kPa. Fig. 9 shows the influence of ΔT_{sub} on $\overline{m}_{L,out}$ and $\overline{m}_V$. For a given heat input value, the larger of $\Delta T_{sub}$is, the smaller $\overline{m}_{L,out}$and $\overline{m}_V$ are. Similar results were found by Bierling et al. (2019) and attributed to the higher location of the first bubble formation in the lift tube when $\Delta T_{sub}$was larger. Rattner and Garimella (2015) also identified the sensitivity of the BPG to the liquid inlet subcooling through simulation.

In fact, the subcooling liquid undergoes two stages in the lift tube: at first stage, the subcooling liquid enters into the lift tube, where it is heated to the saturate and lifted to a certain height under the thermosyphon action. Then in the next stage, the saturated liquid is under continuous heating until boiling to generate vapor bubbles. Thus, the flow pattern evolves along the height, i.e., transition from the bubble flow to the slug flow, churn flow, and annular flow gradually, depending on the heat input. At the stage, the working fluid is lifted effectively under the dual action of bubble pump and thermosyphon, and finally to the vapor-liquid separator. Thus, the second stage is more powerful in terms of the lifting ability and is much more favorable in the design and operation. When the inlet subcooling level remains lower (closer to the phase-change state), the working fluid spend a shorter period at the first stage and experiences more time at the second stage leading to better performance, i.e., both the lifted liquid mass flow rate and the vapor generation rate are higher.

Fig. 10 shows the flow pattern evolution with different ΔT_{sub}, while the heat input was maintained the same (310 W). In general, at a higher inlet subcooling, e.g., 45 °C or 35 °C from phase change, the vapor generation was smaller and rose slowly, thus the outline of vapor bubble was clear. As the inlet subcooling decreased, e.g., 25 °C or 15 °C from phase change, the vapor generation increased and rose faster. Meanwhile, the vapor bubbles and liquid slugs began to oscillate, and the flow pattern gradually changed from slug flow to churn flow. When the inlet subcooling was about 8 °C, large amount of vapor generated and rose even faster, thus liquid slugs and vapor bubbles oscillated more violently, appearing the characteristics of churn flow. Similar flow pattern transitions could also be observed in the case of heating input 530 W and 700 W.

Fig. 11 compares the transient liquid flow curve at different inlet subcooling, while the heat input was the same, i.e., 310 W. At higher inlet subcooling, e.g., 35 °C, the lifted liquid flow was unstable with drastic fluctuation, sometimes the flow stagnation occurred. At lower inlet subcooling, e.g., 8 °C, the flow fluctuation was gentle, while the liquid lifted ability apparently increased.

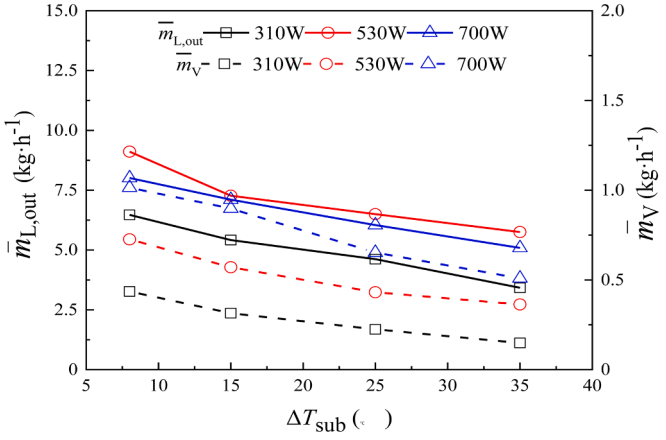

Fig. 9. Effect of inlet subcooling on the BPG performance (P_{sys} = 100 kPa, H = 660 mm)

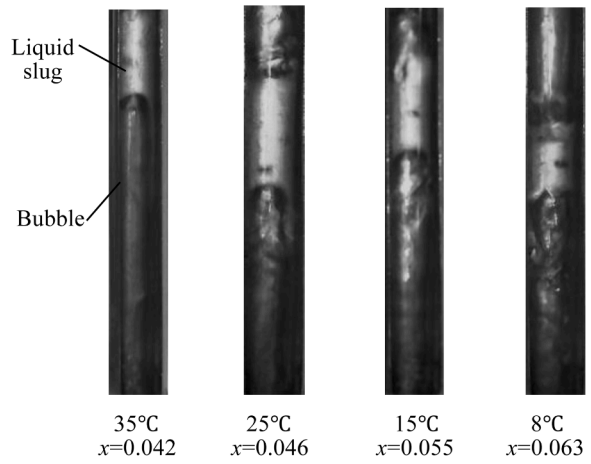

Fig. 10. Flow patterns evolution with different inlet subcooling (8 mm × 80 mm for each size) (P_{sys} = 100 kPa, H = 660 mm, Q_{BPG} = 310W)

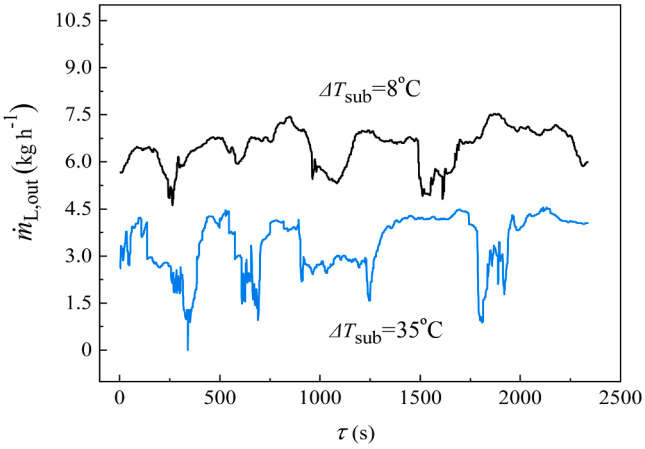

Fig. 11. Transient liquid lifted flow rate for different inlet subcooling (P_{sys} = 100 kPa, Q_{BPG} = 310W)

4.4. Effect of system pressure

In this section, the immersion height and inlet subcooling were kept constant, *i.e.*, H=660 mm, ΔT_{sub}=15 °C, the heating power was kept at 310 W, 430W, and 530 W respectively, while the system pressure was changed in the range of 60 kPa to 100 kPa, to analyze its effect on the flow boiling of BPG.

The results are shown in Fig. 12. In the cases of heat input 310 W and 430 W, the BPG had increasing liquid lifted flow and vapor generation as the system pressure decreased. Accordingly, the flow pattern changed gradually from slug flow to churn flow at the outlet of the lift tube. However, the curve of $\overline{m}_{L,out}$ with respect to pressure was more moderate in the case of heat input 530 W due to the fact that the flow pattern at the outlet of the lift tube was basically in the churn flow, which even tending to annular flow at smaller system pressures.

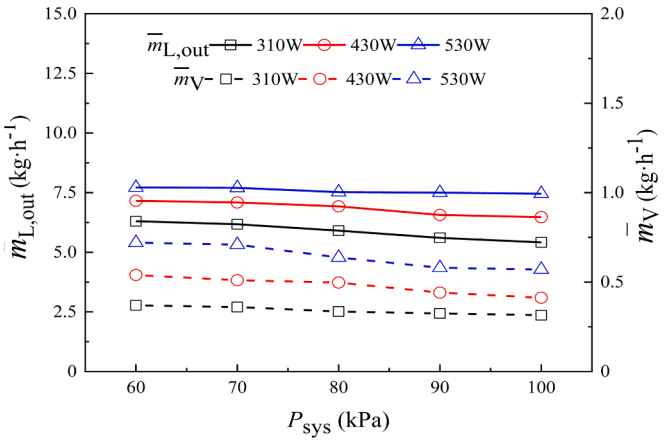

Fig. 12. Effect of system pressure on the BPG performance (H = 660 mm, ΔT_{sub} = 15 °C)

Conclusions

A distribute heating bubble pump generator (BPG) with partial visualization was built to investigate the flow boiling characteristics and pumping performance under the effects of different operational conditions. Detailed experimental studies were conducted over a range of heat input, immersion height, inlet subcooling level, and system pressure. This work is distinct from prior investigations as it incorporated flow visualization and transient flow measurements to explain some of the mechanisms affecting BPG performance. We hope this study to provide some new insights for the bubble pump technology. Here are the main conclusions:

1) Heat input and immersion height were the key factors to determine the flow behavior and lifting performance of the distribute heating BPG. At lower heat input, the flow presented intermittent characteristics and sometimes flow stagnation occurred. As the heat input increased, the fluid flow became more stable, showing higher frequency of oscillation flow and smaller amplitude. Meanwhile the vapor generation increased linearly with the heat input, while the lifted liquid increased at the beginning until a peak and then decreased. Correspondingly, the flow pattern transition was observed at the outlet section of lift tubes, which gradually changed from slug flow to churn flow, and then to annular flow as the heat input increased. The higher of the immersion was, the higher heat input was needed for the flow pattern transition. There existed an optimal heat input for the BPG to lift a maximum amount of liquid, which corresponded to a churn flow regime at the outlet of lift tubes.
2) Liquid lifted process in the BPG was similar to a rising relay, and coupled with a reflux phenomenon, which affected the flow stability and the liquid lifted ability. At higher immersion level, the pumping distance became shorter, which was contributed to the alleviation of reflux, and thus the fluid flow within the lift tubes became more stable and faster. Correspondingly, the liquid lifted ability of the BPG improved, while the vapor generation decreased slightly depending on the inlet subcooling. Moreover, the fluctuation frequency of flow increased while the fluctuation amplitude decreased with the increase of immersion height.
3) Inlet subcooling affected the performance of the BPG. At higher inlet subcooling, the BPG had less vapor generation and poor liquid lifted ability, the fluid flow was unstable and flow stagnation occurred sometimes. At lower inlet subcooling, the BPG could generate more vapor and lift more liquid, which shows better performance. Meanwhile, the flow pattern at the outlet of the lift tubes transited gradually from slug flow to churn flow due to the decrease of inlet subcooling.
4) System pressure also affected the performance of the BPG. With the decrease of system pressure, the BPG generally had increasing liquid lifted ability and vapor generation rate, corresponding to the flow pattern transition gradually from slug flow to churn flow at the outlet of the lift tube. At higher heat input, the variation of the lifted liquid flow rate with the pressure became moderate, and correspondingly, the flow pattern at the outlet of the lift tube was basically in churn flow, even showing tendency to annular flow at smaller system pressure.

This study highlighted the flow pattern evolution in the distribute heating BPG, which determined the flow boiling characteristics and thus the heat and mass transfer mechanism. In addition, the importance of the optimal heat input and the flow stability were identified and needed to be further investigated for the purpose of reliable design and effective operation of the distributed heating BPG.

Declaration of Competing Interest

None.

Acknowledgments

This work was supported by the National Key R&D Program of China (no. 2016YFB0601404).

References

Pfaff, M., et al., 1998. Studies on bubble pump for a water–lithium bromide vapour absorption refrigerator. Int. J. Refrig. 21 (6), 452–462.
Abu-Mulaweh, H., et al., 2011. Design of a bubble pump cooling system demonstration unit. Int. J. Thermal Environ. Eng. 2 (1), 1–8.
Kuo, S.-C., et al., 2013. Bubble pump in a closed-loop system for electronic cooling. Appl. Thermal Eng. 51 (1-2), 425–434.
Han-Shik, C., et al., 2012. Experimental assessment of two-phase bubble pump for solar water heating. J. Central South Univ. 19 (6), 1590–1599.
Jakob, U., et al., 2007. Simulation and experimental investigation into diffusion absorption cooling machines for air-conditioning applications. Appl. Thermal Eng. 28 (10), 1138–1150.
Dammak, N., et al., 2010. Optimization of the geometrical parameters of a solar bubble pump for absorption-diffusion cooling systems. Am. J. Eng. Appl. Sci. 3 (4).
Schmid, F., Spindler, K., 2016. Experimental investigation of the auxiliary gas circuit of a diffusion absorption chiller with natural and forced circulation. Int. J. Refrig. 70, 84–92.
Sayadi, Z., et al., 2013. Performance optimization of solar driven small-cooled absorption–diffusion chiller working with light hydrocarbons. Energy Convers. Manag. 74, 299–307.
Aman, J., Henshaw, P., Ting, D.S.K., 2019. Enhanced exergy analysis of a bubble-pump-driven LiCl-H_2O absorption air-conditioning system. Int. J. Exergy 28 (4), 333–354.
Siyoung, et al., 1998. Pumping characteristics of a thermosyphon applied for absorption refrigerators with working pair of LiBr/water. Appl. Thermal Eng.
Garma, R., et al., 2014. Numerical investigations of the heating distribution effect on the boiling flow in bubble pumps. Int. J. Hydrogen Energy 39 (27), 15256–15260.
Bierling, B., Schmid, F., Spindler, K., 2019. Influence of different heating types on the pumping performance of a bubble pump. Heat Mass Transf. 55 (1), 67–79.
Rattner, A.S., Garimella, S., 2015. Coupling-fluid heated bubble pump generators: experiments and model development. Sci. Technol. Built Environ. 21 (3), 332–347.
Zhang, L., et al., 2006. An experimental investigation on performance of bubble pump with lunate channel for absorption refrigeration system. Int. J. Refrig. 29 (5), 815–822.
Aman, J., Henshaw, P., Ting, D.S.K., 2018. Performance characterization of a bubble pump for vapor absorption refrigeration systems. Int. J. Refrig.-Revue Int. Du Froid 85, 58–69.
Gartia, M.R., Vijayan, P.K., Pilkhwal, D.S., 2006. A generalized flow correlation for two-phase natural circulation loops. Nucl. Eng. Des. 236 (17), 1800–1809.
Benhmidene, A., et al., 2011. Numerical prediction of flow patterns in bubble pumps. J. Fluids Eng. 133 (3), 031302.
Franco, A., Filippeschi, S., 2013. Experimental analysis of closed loop two phase thermosyphon (CLTPT) for energy systems. Exp. Thermal Fluid Sci. (Exp Therm Fluid Sci) 51, 302–311.
Rattner, A.S., Garimella, S., 2018. Simulation of Taylor flow evaporation for bubble-pump applications. Int. J. Heat Mass Transf. 116, 231–247.
Trinh, Q.D., et al., 2019. Operational behavior and heat transfer in a thermosiphon desorber at sub-atmospheric pressure. Part I: the model. Int. J. Refrig.-Revue Int. Du Froid 108, 246–257.

Benhmidene, A., et al., 2016. Experimental investigation on the flow behaviour in a bubble pump of diffusion absorption refrigeration systems. Case Stud. Thermal Eng. 8, 1–9.
Jo, S.W., Lear, W.E., Sherif, S.A., 2014. Numerical simulation of saturated flow boiling heat transfer of ammonia/water mixture in bubble pumps for absorption-diffusion refrigerators. J. Thermal Sci. Eng. Appl.: Trans. ASME.
Han, X.H., et al., 2015. Experimental investigations on the pumping performance of bubble pumps with organic solutions. Appl. Thermal Eng. 86, 43–48.
Koyfman, A., et al., 2003. An experimental investigation of bubble pump performance for diffusion absorption refrigeration system with organic working fluids. Appl. Thermal Eng. 23 (15), 1881–1894.
Ben Ezzine, N., et al., 2010. Experimental studies on bubble pump operated diffusion absorption machine based on light hydrocarbons for solar cooling. Renew. Energy 35 (2), 464–470.
Benhmidene, A., Chaouachi, B., 2019. Investigation of pressure drop in the bubble pump of absorption-diffusion cycles. Appl. Thermal Eng. 161.
Belman-Flores, J., et al., 2014. Energetic analysis of a diffusion–absorption system: A bubble pump under geometrical and operational conditions effects. Appl. Thermal Eng. 71 (1), 1–10.
Delano, A.D., Design analysis of the Einstein refrigeration cycle. 1998.
White, S.J., 2001. Bubble Pump Design and Performance. School of Mechanical Engineering, Georgia Institute of Technology.
Chisholm, D., 1985. Two-phase flow in heat exchangers and pipelines. Heat Transf. Eng. 6 (2), 48–57.
Lin, F., et al., 2016. An experimental study on the performance of guided bubble pump with multiple tubes. Appl. Thermal Eng. 106, 1052–1061.
Vicatos, G., Bennett, A., 2007. Multiple lift tube pumps boost refrigeration capacity in absorption plants. J. Energy South. Afr. 18 (4), 49–57.
Gurevich, B., et al., 2015. Performance of a set of parallel bubble pumps operating with a binary solution of R134a-DMAC. Appl. Thermal Eng. 75, 724–730.
O'Neill, L.E., Mudawar, I., 2020. Review of two-phase flow instabilities in macro- and micro-channel systems. Int. J. Heat Mass Transf. 157.
Ham, S., Choi, S., Jeong, J.H., 2021. Two-phase flow distribution in a refrigerant distributor having four indoor-unit connections of a variable refrigerant flow system. Int. J. Refrig. 126, 246–258.
Ruspini, L.C., Marcel, C.P., Clausse, A., 2014. Two-phase flow instabilities: a review. Int. J. Heat Mass Transf. 71, 521–548.
Lemmon, E., et al., 2018. NIST Standard Reference Database 23: Reference Fluid Thermodynamic and Transport Properties-REFPROP, Version 10.0. National Institute of Standards and Technology. Standard Reference Data Program, Gaithersburg.
Handbook-Fundamentals, A., American society of heating. refrigerating and air-conditioning engineers, 2009.
Moffat, R.J., 1988. Describing the uncertainties in experimental results. Exp. Thermal Fluid Sci. 1 (1), 3–17.
Yeboah, S.K., Darkwa, J., 2018. Thermal performance of a novel helically coiled oscillating heat pipe (HCOHP) for isothermal adsorption. An experimental study. Int. J. Thermal Sci. 128, 49–58.
Halimi, M., Nejad, A.A., Norouzi, M., 2017. A Comprehensive experimental investigation of the performance of closed-loop pulsating heat pipes. J. Heat Transf.-Trans. Asme 139 (9).
Benhmidene, A., et al., 2011. Modelling of heat flux received by a bubble pump of absorption-diffusion refrigeration cycles. Heat Mass Transf. 47 (11), 1341–1347.
Chan, K.W., McCulloch, M., 2013. Analysis and modelling of water based bubble pump at atmospheric pressure. Int. J. Refrig. 36 (5), 1521–1528.